

A robust and omnidirectional-sensitive electronic antenna for tactile-induced perception

Received: 16 November 2024

Accepted: 18 March 2025

Published online: 01 April 2025

Hao Ren ^{1,2}, Liu Yang ^{2,3,4}, Hong-yuan Chang ², Tieshan Zhang ², Gen Li², Xiong Yang², Yifeng Tang¹, Wanfeng Shang ⁵ & Yajing Shen ^{2,6} 

Skin-like planar tactile sensors have achieved adaptive gripping, in-hand manipulation, and human-machine interaction but remain limited in tasks requiring active environmental interaction and robustness against large mechanical perturbations. Inspired by the biological antennas of nocturnal insects, we introduce a biological antenna-like electronic tactile sensor with enhanced mechanical robustness, capable of withstanding 1800% twist, 224% stretch, 360° bending, large compression, and punctures. Through segmented flexibility and partial magnetization, it achieves an impressive 1.76° omnidirectional loading recognition accuracy, outperforming biological antennas by 17 times. Its scalable plug-and-play capability, combined with a tactile perception algorithm, ensures seamless integration across various robots for diverse tasks. We demonstrate the vision-free navigation with 0.2 mm tracking deviation, 97% accuracy in ground texture recognition, and conformal robotic brushing on serpentine surfaces with a force variance of 0.34 N. This research offers valuable insights for active tactile-based environmental perception and interaction, promising advancements in robotics across various fields.

Biological organisms rely heavily on touch for both passive and active interactions with their environment. While passive tactile sensing detects stimuli resulting from skin deformation, active tactile sensing involves probing the environment using specialized sensors or organs like antennae, whiskers, and fingertips. At present, various types of electronic skins have been developed based on diverse working principles, such as piezoresistive^{1,2}, capacitive³, ionic⁴, transistor-based⁵, magnetic⁶, triboelectric nanogenerator (TENG)^{7,8}, optic^{9–11}, etc, exhibiting high spatial and force resolution akin to biological skin¹². However, the complex wiring, restricted deformation, and limited robustness to damage from substantial mechanical perturbations reduce their suitability for direct environmental interaction.

As a supplement, organisms also utilize cilia-like tactile organs with slender structures for tactile sensing. These organs offer increased sensitivity, high mechanical compliance and omnidirectional discrimination, enabling the perception of subtle cues and active exploration of surroundings. For instance, embryos use cilia to sense fluid flow direction^{13,14}, and insects use antennae to probe surfaces to detect textures and shapes of objects¹⁵. As for artificial cilia-like sensors, current solutions can be divided into three types based on the transducer principles, electric, photonic, and magnetism. Electric-based sensors, such as those described in refs. 16,17, are effective for passive tasks like flow speed and pressure sensing. However, their inherently one-dimensional nature limits their capability for

¹The Robot and Automation Center and the Department of Biomedical Engineering, City University of Hong Kong, Hong Kong SAR, China. ²Department of Electronic and Computer Engineering, The Hong Kong University of Science and Technology, Hong Kong SAR, China. ³National Key Laboratory of Intelligent Tracking and Forecasting for Infectious Diseases, Tianjin Key Laboratory of Intelligent Robotic, Institute of Robotics and Automatic Information System, Nankai University, Tianjin, China. ⁴Institute of Intelligence Technology and Robotic Systems, Shenzhen Research Institute of Nankai University, Shenzhen, China.

⁵Shenzhen Institutes of Advanced Technology, Chinese Academy of Sciences, Shenzhen, China. ⁶Center for Smarting Manufacturing, The Hong Kong University of Science and Technology, Hong Kong SAR, China. ✉ e-mail: eeeyajing@ust.hk

directional discrimination. While advancements like MEMS structures incorporating four pairs of strain gauges¹⁸ have been introduced to enhance direction-sensing capabilities, these approaches are still constrained by the limited deformation range of MEMS structure. Photonic-based sensors¹⁹ offer high sensitivity and can detect weak signals, but they also face challenges in multi-directional discrimination and mechanical robustness. Magnetic-based solutions have explored approaches such as mounting polarized magnets on rotatable bases for directional transduction^{20,21}. However, these systems are typically limited by a restricted rotation range ($\sim 20^\circ$) and accuracy constraints. Other methods, including those leveraging giant magneto-impedance²² or electromagnetic induction effects^{20,21}, have shown promise for vibration sensing and human-machine interaction. However, achieving a combination of high sensitivity, mechanical robustness, and omnidirectional sensing remains a significant challenge for bio-mimic cili/whisker-like tactile sensors. Moreover, the absence of sophisticated post-processing algorithms limits these sensors' ability to deliver meaningful environmental perception for robotic applications.

Here, we present an electronic antenna system (E-Antenna) inspired by the flexible antenna and the tactile mechanism of nocturnal insects (Fig. 1A). Similar to insects' antenna, the antenna can convert stimuli into tactile signals through its deformation. Firstly, we demonstrated the adoption of partial magnetization and segmented flexibility can enhance its tactile sensitivity and omnidirectional sensing capabilities. Secondly, we illustrated that its non-wired magnetic sensing principle and cantilever-like structure provide robustness against mechanical perturbations. Then, combined with the proposed sequential tactile perception method, the scalable E-Antennas were integrated into various robotic platforms and verified its efficacy in enhancing mobile robots with ground texture perception ability, aiding mobile robots' navigation in dark environments, enabling robot arms to execute intricate manipulations on curved surfaces. We foresee that the E-Antenna will significantly enhance the tactile sensing and environmental perception capabilities of robots, catalyzing advancements in intelligent perception, navigation and manipulation in complex environments.

Results

Principle, design, and fabrication of the biomimetic electronic antenna

Nocturnal insects/animals with degraded vision have evolved a high-sensitive antenna/whisker system that can actively explore and extract environmental information through touch^{23,24}, such as the active wall-following behavior of cockroaches in a dark environment by their antennae²⁵ (Fig. 1A). Inspired by the overall mechanism of nocturnal insects' perception, which involves antennal mechanosensing, neural signals transmission, tactile information decoding in the brain, and somatic motion control, we propose an electronic antenna sensory system (Fig. 1B). The basic sensing principle of it is that the E-Antenna senses external stimuli by deforming, which alters the magnetic field and causes variations in the underlying multidimensional magnetometer readings.

The artificial antenna is designed to be slender (scalable) with a partial magnetization strategy and diverse flexibility configuration (Fig. 1C). The distal segment of the antenna is made of DragonSkin 20 (E - 1.1 MPa) and partially embedded with NdFeB magnetized nanoparticles (50 wt%) that serve as system mechanoreceptors. The proximal substrate of the antenna is made of Ecoflex 0030 with a smaller Young's modulus of -115 kPa. The overall weight of the millimeter-scale antenna is -44 mg. A tiny three-axis magnetometer ($2.5 \times 3 \times 0.86$ mm) is assembled underneath the antenna to convert its deflection and orientation into quantitative electrical signals. Subsequently, a compact wireless circuit board ($23 \times 40 \times 2$ mm) is developed to transmit signals in real-time, replacing the neural conductive pathway of a

biological antenna. More details about the fabrication are given in the methods section.

By incorporating the E-Antenna, the robots can gain the ability to actively engage with their surroundings. Unlike conventional tactile sensors primarily used for force or pressure measurement, the E-Antenna can extract additional information, such as object properties and contact dynamics, through a sequential observation chain $[\mathbf{B}_{t-n}, \mathbf{B}_{t-n+1}, \dots, \mathbf{B}_t]$. This temporal information, coupled with the developed lightweight sequential AI model, empowers the robot to comprehend its environment, enhance perception, and execute more advanced tasks (Fig. 1D, E).

Theoretical modeling and optimization by partial magnetization and segmented flexibility configuration

As illustrated in Fig. 2A-i, the biological antenna has features of a slender flagellum. The E-Antenna is modeled in cylindrical coordinates for a better illustration of the stimuli direction (Fig. 2A-ii, Fig. S1). Then, the deflected antenna can be considered as an elastic spring-hinged cantilever beam on the surface (X'OY') parallel to the force direction (Fig. 2A-iii).

$$EI \frac{d^2\phi}{ds^2} + F \sin(\phi + \lambda) = 0, \text{ s.t. } \kappa(0) = 0, -EI\kappa(l) + c\phi_1 = 0, \quad (1)$$

symbolized as $\phi = f(F|EI, c)$

where EI represents the flexural rigidity, l represents the length, $0 \leq s \leq l$ is the arc length measured from the free end to its fixed end, ϕ is the tangent angle, z is the curve curvature, λ is the force inclination angle, and c is the rotational spring stiffness of the substrate.

Because the robotic antenna was magnetized uniformly along the axis, $\mathbf{M} = (0, 0, M_0)$, the following boundary conditions hold: $\nabla \cdot \mathbf{M} = 0$ inside the antenna, $\vec{B} = 0|_{\vec{r} = \infty}$, and $\text{div}(\mathbf{M})|_{S_t} = -M_0$, $\text{div}(\mathbf{M})|_{S_b} = M_0$ on the two end surfaces. Thus, the magnetic flux intensity measured by the Hall sensor can be represented as (the formula derivation process in the supplementary file).

$$\mathbf{B}(\mathbf{r}) = -\mu_0 \nabla \left[-\frac{1}{4\pi} \int_{S_t} \frac{M_0}{|\mathbf{r} - \mathbf{r}'_t|} dS - \frac{1}{4\pi} \int_{S_b} \frac{M_0}{|\mathbf{r} - \mathbf{r}'_b|} dS \right] \quad (2)$$

where μ_0 is vacuum permeability, \mathbf{r} represents the position vector of the measurement point, \mathbf{r}'_t and \mathbf{r}'_b represent the position vector of the point on the top surface and bottom surface, respectively, S_t and S_b represent the top surface and bottom surface of the antenna. Thus, for a specific deflection, the \mathbf{B} at the magnetometer position \mathbf{P} can be derived and symbolized as (see modeling in supplementary material):

$$\mathbf{B} = G(\alpha, \gamma, H, L | (\mu_0, M_0, H_0, R)) \quad (3)$$

where α is the angle between the projection of the antenna on the XOY plane and the X-axis, γ is the cumulative deflection angle of the free end, L and H represent the central position of the free end in the YOZ plane of the antenna coordinate frame. According to the deformation-magnetism observation model (Eq. 1) and force-deformation model (Eq. 3), the deflection state and the applied force (including both the magnitude and orientation) can be mapped by the magnetism observation \mathbf{B} .

To improve the sensitivity under a specific magnetization strength M_0 , we further optimized the structure of the antenna based on its working principle. Referring to the representation of sensing sensitivity

$$S = \frac{\partial \overline{\Delta B}}{\partial P} = \frac{\partial \overline{\Delta B}}{\partial L} \frac{\partial L}{\partial P} = S_m * S_L \quad (4)$$

where $\overline{\Delta B} = (B - B_0)/B_0$ is the normalized magnetic strength change, L is the deflection, P is the load applied on the antenna, $S_m = \partial \overline{\Delta B} / \partial L$ and

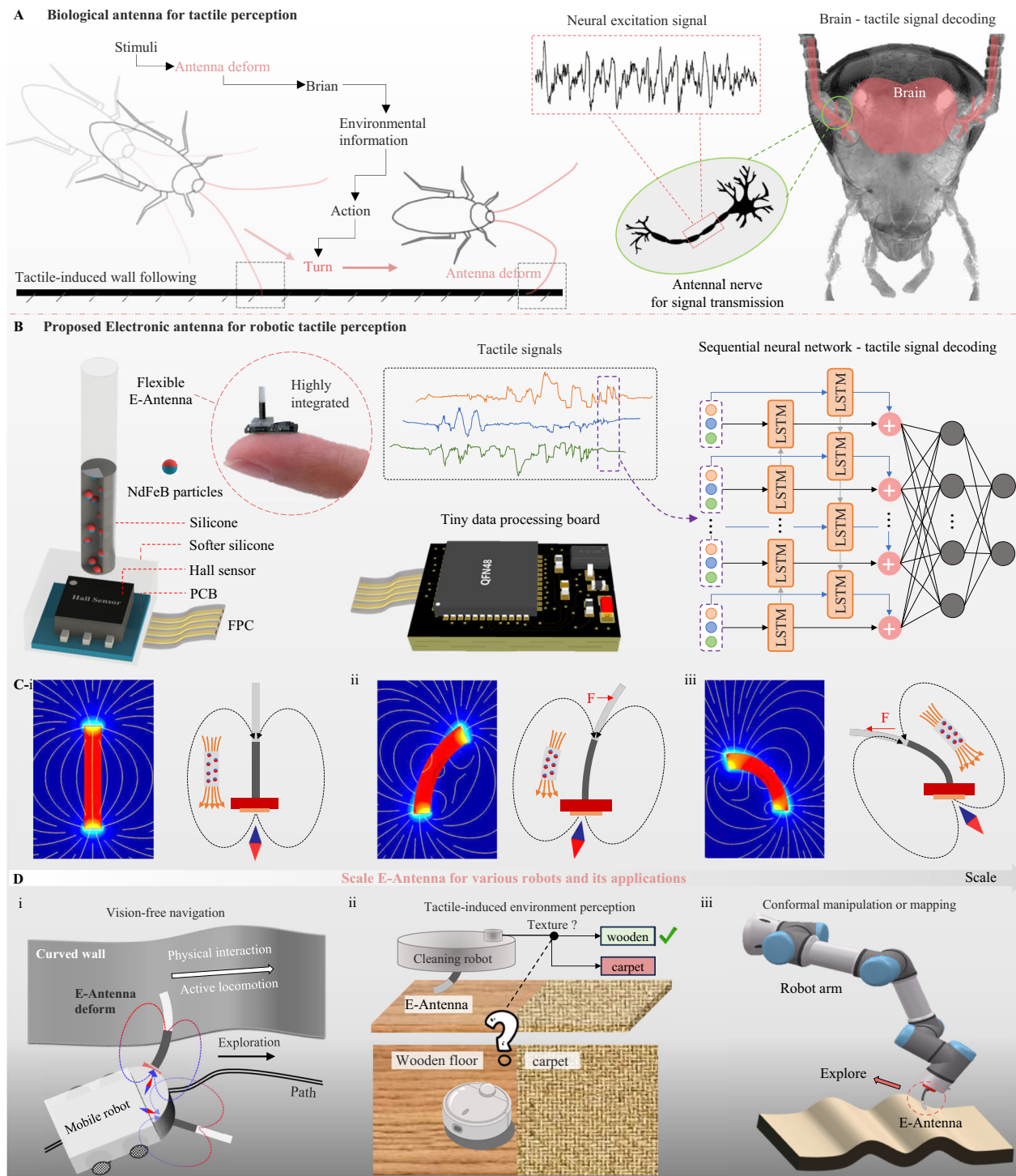


Fig. 1 | Illustration of the bioinspired flexible electronic antenna (E-Antenna) for robots tactile perception. **A** The schematic of insect's vision-free wall-following navigation behavior: The insect's antenna converts mechanical stimuli from its surroundings into neural signals through deformation, allowing the brain to extract environmental information from tactile input to guide its locomotion. **B** The proposed bioinspired E-Antenna sensory system with a highly integrated design, featuring a flexible artificial antenna with partial magnetization and segmented flexibility, a compact data processing board, and a sequential neural network for tactile perception. **C** Illustration of E-Antenna's fundamental sensing principle: similar to the biological antenna, the artificial antenna utilizes

deformation to sense the direction and magnitude of applied loads. (i) The unloaded state of the antenna and the original magnetic field distribution; (ii) Antenna deforms under a load, resulting in the deflection of its magnetic field; (iii) A larger load in the opposite direction leads to a greater reverse deflection of the magnetic field. **D** E-Antenna can be made in multiple scales for different robots and applications: (i) Mounting of a centimeter-scale E-Antenna on a mobile robot for insect-like vision-free wall-following navigation; (ii) Integration of a millimeter-scale E-Antenna in a cleaning robot for floor classification via tactile texture perception; (iii) Incorporation of a larger E-Antenna into robotic arms for conformal manipulation or surface mapping.

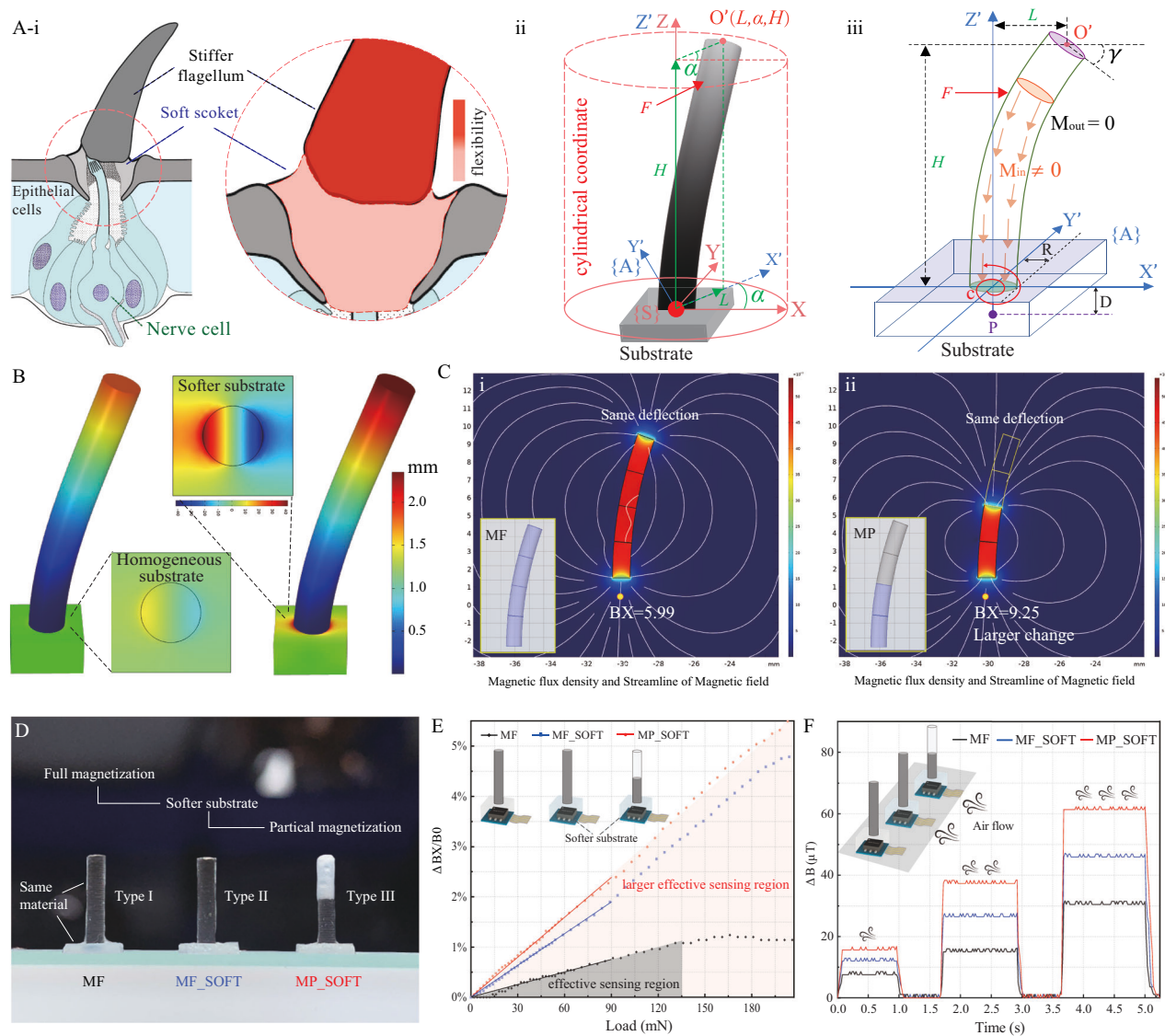


Fig. 2 | Design, modeling, and optimization of the E-Antenna. **A** E-Antenna's design philosophy: (i) Schematic diagram of the biological antenna with slender flagellum and segmented stiffness distribution; (ii) E-Antenna modeling in cylindrical coordinates, featuring an insect-like slender structure and a uniform cylindrical shape; (iii) Force mode of the E-Antenna on the plane parallel to the force direction. **B** Strain simulation of antennas with a softer and standard substrate under the same load. **C** Simulation results of the magnetic field of the full-magnetized antenna and partial-magnetized antenna with the same deflection angle, respectively. **D** Photographs of E-Antennas with different designs, the left

(MF) is a basic homogeneous design with full magnetization and normal substrate, the middle design (MF_SOFT) adopts a softer substrate, and the right design (MP_SOFT) further takes partial magnetization strategy. **E** The static responses of the three E-Antennas under varied loads indicate that the optimized design exhibits higher sensing sensitivity and a larger sensing range. **F** The dynamic responses of the three E-Antennas under three-level air flow showcase that the optimized design enhances the sensing signal-to-noise ratio (SNR) by ~200%, enabling robots to discern subtle features and achieve reliable tactile perception.

$S_L = \partial L / \partial P$ represent the magnetism-to-deflection sensitivity and deflection-to-load, respectively, the sensitivity of the antenna can be increased if the structure can induce a stronger ΔB at a certain deflection and/or generate a larger deflection L under a certain load.

To generate a larger deflection L under a certain load, one direct approach is to use a low-stiffness material (lower E). Yet, employing this strategy for the slender antenna presents challenges in maintaining its initial state against gravitational forces due to the low bending stiffness. Similar to the inhomogeneous stiffness distribution of the insect antenna (Fig. 2A-i)²⁶, our segmented flexibility configuration design, i.e., soft substrate and stiffer antenna, provides mechanical stability against the antenna's own weight and flexibility to external stimuli, ensuring a balance between mechanical robustness and sensitive sensory perception. Simulation results (Fig. 2B) demonstrate that the design with a softer substrate exhibits larger deformation

sensitivity, improving by 205.56% from $1.62 \mu\text{m} \cdot \text{Pa}^{-1}$ to $4.95 \mu\text{m} \cdot \text{Pa}^{-1}$ under 2 mN concentrated load.

To gain a higher S_m , we investigated the effect of the antenna's length on magnetic strength change during deflection. Surprisingly, both theoretical and simulation results imply that a short antenna with full magnetization can generate a larger ΔB at **P** with a certain deflection angle (means a larger magnetism-to-deflection sensitivity S_m) (Fig. S2). However, as the antenna's length decreases, its deflection-to-load sensitivity S_L reduces, which is a side effect on the improvement of the overall sensing sensitivity (S). To address this contradiction, we propose a partial magnetization strategy to shorten the effective magnetization length and improve sensing sensitivity without sacrificing the deflection sensitivity. Simulation results (Fig. 2C-i, ii) show that the half-magnetized antenna exhibits a 54.42% increase compared to the fully magnetized antenna when the deflection angle is 20° .

To verify these optimized design strategies (Fig. S5), we fabricated three antennas with the same length (8 mm) from the same material (DragonSkin 20 with E - 1.1 MPa) but using different magnetization and substrates (Fig. 2D), i.e., fully magnetized (MF), fully magnetized with a soft substrate (MF_SOFT) and 4 mm partially magnetized with a soft substrate (Ecoflex 30 with E - 115 kPa) (PF_SOFT). Load-sensing results (Fig. 2E) show that the antenna with a softer substrate (MF_SOFT) remarkably improves sensitivity by 155.40% from $8.25 \cdot \text{N}^{-1}$ to $21.07 \cdot \text{N}^{-1}$, and the partial magnetization (PF_SOFT) strategy further improves magnetic sensitivity by 26.96% (to $26.75 \cdot \text{N}^{-1}$). Particularly, the optimized design significantly increases sensitivity by approximately 224.24% within a small load range (0–90 mN). Moreover, the optimized design expands the reliable sensing range by ~1.7 times compared to the basic homogeneous design (from 16–120 mN to 0–180 mN), while maintaining excellent linearity ($R^2 = 0.9987$) across the full range.

To further demonstrate the advancement of the optimized design intuitively, we evaluated these sensors by measuring the airflow from a blower 10 cm away. The results indicate that the sensing signal-to-noise ratio (SNR) of the optimized antenna (PF_SOFT) is ~220% higher than the original antenna (MF) (Fig. 2F). This improvement makes the E-Antenna has enhanced discrimination to fine features of external objects, which is crucial for achieving reliable tactile perception. The seamless connection observed in the SEM images between the magnetic and pure-elastomer segments suggests strong interfacial bonding (Fig. S9), contributing to good mechanical strength and durability in the composite material.

Characterization of the E-Antenna's sensing ability, mechanical robustness and physical wound robustness

The static sensing characteristics (Fig. 3A) show that the sensor has a dominant linear sensing range of $[-120, 120]$ mN, with a slope of 40 mN/1%, and exhibits strong multi-directional consistency in force sensing, confirmed by a t-test ($p = 0.9872$). Moreover, the optimized antenna exhibits high accuracy in stimuli direction recognition (Fig. 3B, Movie. S1), with a maximum STD of 1.76° at 135° orientation and a minimum STD of 0.13° at 180° orientation (Fig. 3C), ~17 times better than the -30° direction recognition performance of reported insect tactile organs²⁷. We also characterized the E-antenna's dynamic response, including amplitude, waveform, and frequency characteristics. It exhibits a nearly linear magnitude response to dynamic stimuli ($k = 2.23\% \cdot \text{mm}^{-1}$, $R^2 = 0.9979$), accurately tracking the triangle and square wave stimuli (Fig. 3D). Additionally, it shows a consistent and discernible response to varying frequencies (Fig. 3E), confirmed by a group analysis of variance with significant results ($P < 0.0001$) and residual within-group value of 0.0036. Moreover, the antenna also demonstrates good durability, remaining stable over 3500 tails (Fig. 3F).

The E-Antenna also exhibits notable mechanical and wound robustness, demonstrating an exceptional ability to recover from substantial physical stimuli without compromising its functionality (Fig. 3G). One standout feature is its capacity to recover from a 1800° twist (Fig. 3G-i, Movie. S2), allowing it to maintain operational integrity in dynamic environments with significant torsional forces that typically damage conventional planar flexible tactile sensors. Additionally, the E-Antenna can endure a 224% stretch (Fig. 3G-ii, Movie. S2), withstand nearly 360° bending (Fig. 3G-iii, Movie. S2), and sustain compressive force far exceeding its own weight ($\sim 2.28 \times 10^6$ times self weight, 100 kg vs 44 mg, Fig. 3G-iv, Movie. S3). Moreover, its non-wired, magnetism-based sensing mechanism enhances its resistance to physical damage. For instance, as shown in Fig. 3G-v, Fig. S10 and Movie. S4, the antenna recovered both its morphology and functionality after needle punctures (seven random puncture positions). It can also continue functioning even after being cut and can be quickly repaired with glue in a few minutes for emergency usage (Fig. S11). The recovery

factor of the repaired E-Antenna for stretching is approximately 20%, while for torsion and compression, it is around 40%. Moreover, the E-Antenna also can be used underwater after encapsulating with insulating sealant silicone (Fig. S12). If mechanical interference exceeding the above-mentioned tolerance is applied, the E-Antenna may undergo irreversible deformation or breakage.

The E-Antenna's mechanical and damage robustness enables it to withstand harsh conditions, substantial deformation, and physical impacts without losing functionality. This reliable resilience, along with its improved sensing performance, makes it ideal for practical robotic demanding systems, providing durable and reliable sensing even suffering substantial mechanical perturbations.

Tactile perception strategy based on sequential sensing observation chain

Insects and animals possess intelligent perception ability upon tactile stimuli. However, reproducing this sophisticated perception in engineering remains challenging^{28,29}, largely due to the predominant reliance on passive sensing methods and the lack of efficient techniques for extracting and interpreting tactile information. To tackle this issue, we propose an active tactile perception method (ATPM) inspired by the active touch mechanism observed in biological organisms.

To begin, akin to the active tactile exploration observed in biological antennae, the E-Antenna actively engages with objects to capture a richer array of spatial features (Fig. 4A). Subsequently, a sliding window is employed to dynamically construct a sensing observation chain $[\mathbf{B}_{t-n}, \mathbf{B}_{t-n+1}, \dots, \mathbf{B}_t]$ that retains temporal dependencies and contextual information of contact events. This chain is then fed into a multi-layer sequential neural network for perception analysis. The neural network is structured with hierarchical feature extraction and non-linear feature fusion capabilities, comprising of a sequential input sensory layer, a bi-directional long short-term memory (LSTM) backbone for initially extracting underlying features, a unidirectional LSTM layer for further extracting and fusing contextual features, and two fully connected (FC) branches for final feature fusion and prediction (One identifies the state of the robotic antenna, and the other predicts environmental features). This design facilitates the effective processing of raw tactile signals and the extraction of temporal-spatial features, along with contextual information.

To evaluate its capability for tactile perception, we selected the most challenging tactile curvature perception task requiring both accurate sensing and effective interpreting abilities. The electronic antenna swept across five curved surfaces, and its recognition results were recorded and analyzed (the detailed surface information and raw sensing data shown in Fig. S13). The classification confusion matrix (Fig. 4B) demonstrates high self-state recognition accuracy, with most states exhibiting perfect discrimination accuracy of 100%. Even for states 2 and 3 involving smooth transitions from planar to curved parts, the ATPM still exhibits a high classification accuracy of 93%. Additionally, the ATPM demonstrates notable performance in curved surface perception (Fig. 4C), achieving high-precision curvature perception with an average estimation error of less than 0.9° , surpassing human haptic curvature discrimination performance of 5.3° ³⁰ and overcoming limitations of conventional passive tactile methods in complex geometry perception. It's worth noting that the proposed ATPM is effective for various other environment perceptions, such as surface roughness recognition and surface topology perception (Fig. S14). This accurate and reliable perceptual ability enable achieving challenging tasks in versatile robotic systems, including but not limited to robot arms, mobile robots, and healthcare devices.

Scalable E-Antenna functionalized various robots with tactile-perception capabilities

Tactile sensing is a crucial tool for living organisms, enabling effective navigation and environmental perception, especially when visual

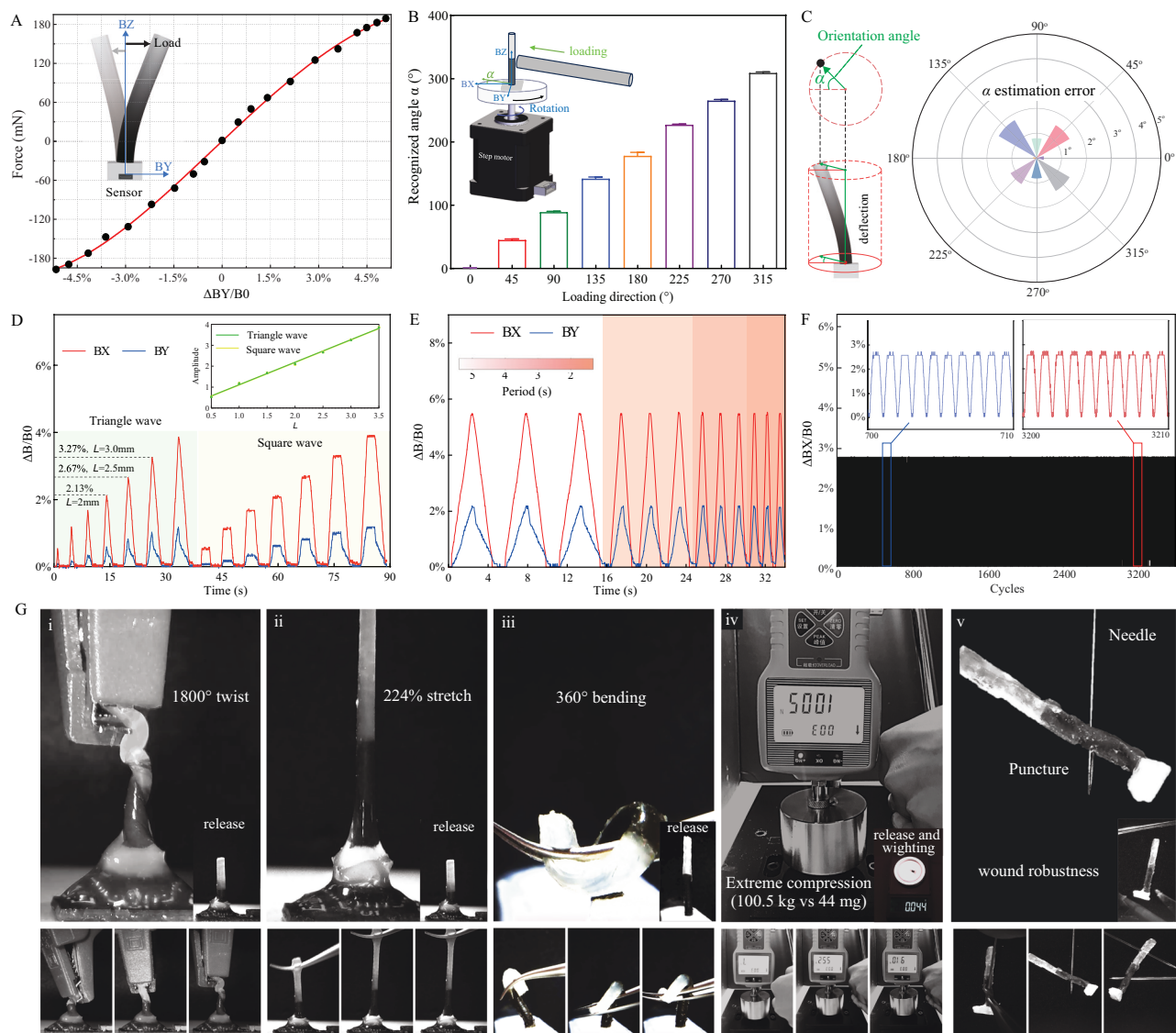


Fig. 3 | The sensing characterization and mechanical robustness of the E-Antenna. **A** The consistent responses of the E-Antenna to bidirectional loads. **B** The loading direction recognition performance of the E-Antenna across eight loading directions. **C** The statistic analysis of prediction direction (α) error, where the maximum standard deviation (STD) is 1.76° . **D** Dynamic responses of the E-antenna under two kinds of dynamic loading with increasing loading amplitudes. **E** Dynamic responses of the E-Antenna under loads with increasing frequency.

F Stability validation over 3500 trials, indicating the E-Antenna has reliable and consistent tactile sensing ability. **G** Demonstrations of the mechanical robustness and physical wound robustness of the E-Antenna (i and ii are millimeter-scale, iii, iv, and v are centimeter-scale), highlighting its ability to recover from 1800° twist, 224% stretch, 360° deflection, sustain up to 10^3 N of compression (~ 100 kg vs 45 mg), and even needle punctures.

sensing is unavailable or inefficient. For instance, wall-following behavior is vital for nocturnal animals, providing a defined path that aids in navigation and reduces vulnerability to predators. Our E-Antenna enhances the tactile sensing capabilities of mobile robots, serving as a valuable complement to existing vision-based navigation systems. Here, we showcase the E-Antenna's ability to facilitate insect-like wall-following locomotion in mobile robots (Movie. S5).

As depicted in Fig. 5A, we designed a small mobile robot equipped with two E-Antennas (2 mm in diameter and 20 mm in length) on its head. The E-Antenna system provides real-time contact and distance information based on its deformation, guiding the robot to navigate along a serpentine wall (Fig. 5B). This wall features a concave section, a near-linear segment, and a convex section, encompassing both common and challenging geometric features in navigation maps.

Fig. 5C shows that the robot's trajectory during wall-following closely matches the wall's serpentine outline, demonstrating its

effectiveness in following the wall throughout all segments. Analysis of the robot's steering angle reveals that its variation and spatial distribution (red line in Fig. 5D) are consistent with the tangent angle of the wall's outline. Specifically, as the robot passes the concave section, its steering angle shifts from -32° to 23° . In the convex section, the angle transitions from 20° , crosses 0° , and decreases to -19° . This indicates that the E-Antenna guided the robot dynamically adjusts its direction to maintain contact with the wall, which provides stable contact signals (Fig. 5E). Consequently, the distance between the mobile robot and the wall fluctuates within a small deviation of 2.04 mm (1/20 of the robot's width), and reducing the robot's speed can further improve tracking accuracy (Fig. S15). This biomimetic wall-following navigation strategy offers valuable insights into robotic navigation in scenarios where visual information is unavailable, particularly in unfamiliar and dark environments.

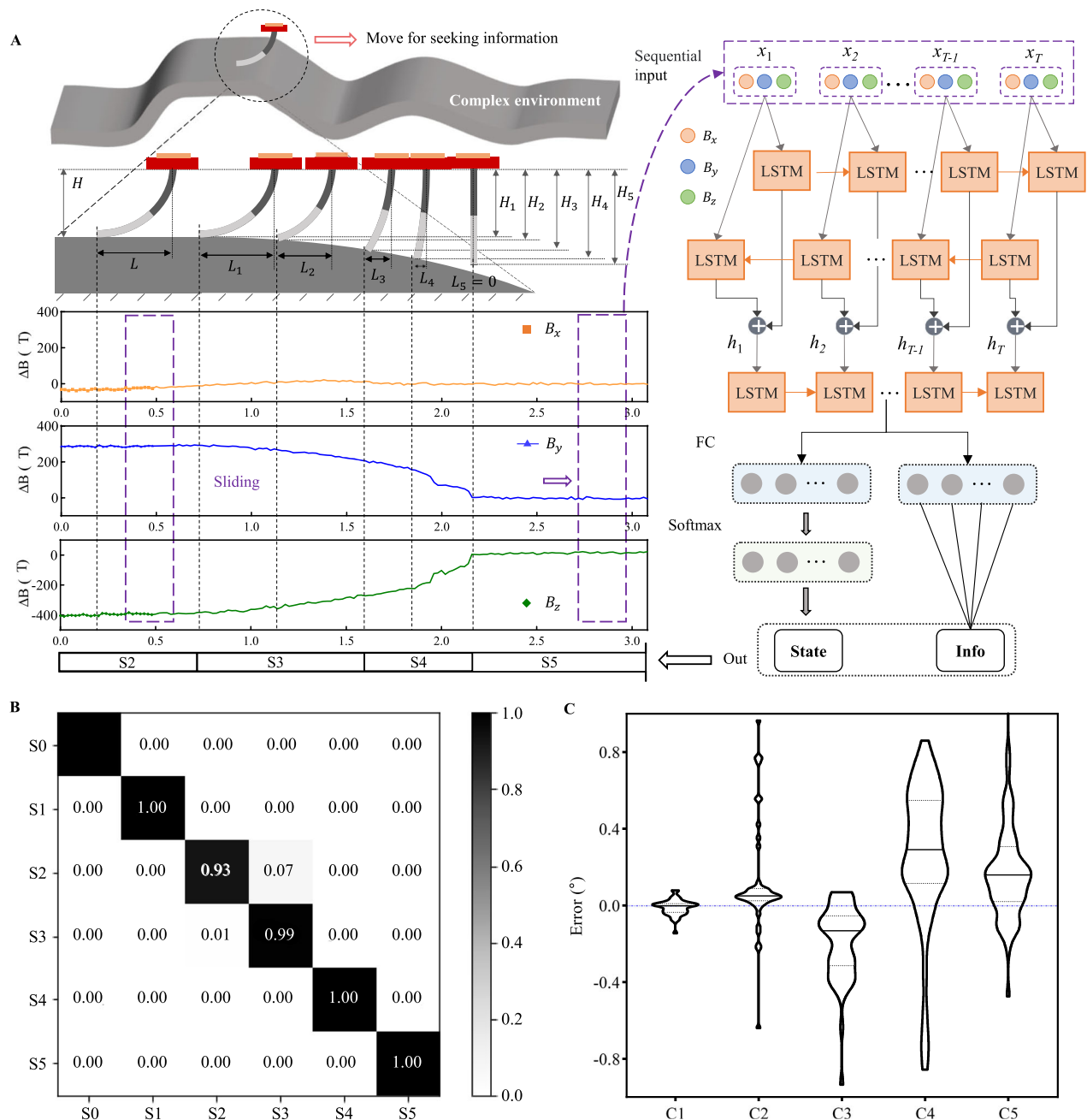


Fig. 4 | AI-assisted active tactile perception strategy and validation.

A Schematic of active tactile perception strategy. The E-Antenna is moved to interact with objects for gathering time-spatial features along the moving direction, a sliding window is used to integrate discrete tactile signals to construct a tactile sensing sequence, and a sequential neural network is designed to perceive

environmental information and the antenna's state. **B** Confusion matrix of the classification results of antenna's states (S0-S5) where most classes achieve 100% classification accuracy. **C** Violin plot of the prediction error for five surfaces with varying curvatures (C1: 40°, C2: 61°, C3: 62°, C4: 63°, and C5: 65°), where the overall maximum error is less than 1°.

Another common challenge faced by existing mobile robots is the perception of ground texture, particularly for home-cleaning robots³¹. This always causes ineffective cleaning and potential damage to delicate floors. Functionalizing cleaning robots with texture perception can intelligently adopt the optimal cleaning strategy for different surfaces (Fig. 6A). We demonstrate our e-antenna provides a solution to this challenge (Movie S6). As depicted in Fig. 6B, we mounted the E-Antenna (0.9 mm in diameter, 9 mm in length) on the underside of a mobile robot to functionalize it with ground texture perception capability. We selected three types of flooring commonly used in households: wooden floors, ceramic tiles, and carpets (Fig. 6C). As shown in Fig. 6D, with the movement of the robots, the tactile signals fluctuate

the most on the carpet due to its coarse surface, while ceramic is the least owing to its smooth surface. Despite the visual similarities between ceramic floors with wood-like patterns and genuine wooden floors, the tactile signals from wooden floors exhibit greater fluctuations than compared to those from ceramic tiles. This aligns with the fact that ceramic tiles have a smooth glaze (enamel) layer while wooden floors feature coarser natural grain.

Further, we processed the raw sequential tactile signals using the ATPM to extract the high-level features, which are then visualized with the t-distributed Stochastic Neighbor Embedding (t-SNE) method. The results (Fig. 6E) reveal three distinct clusters, indicating a clear separation of tactile features across the three

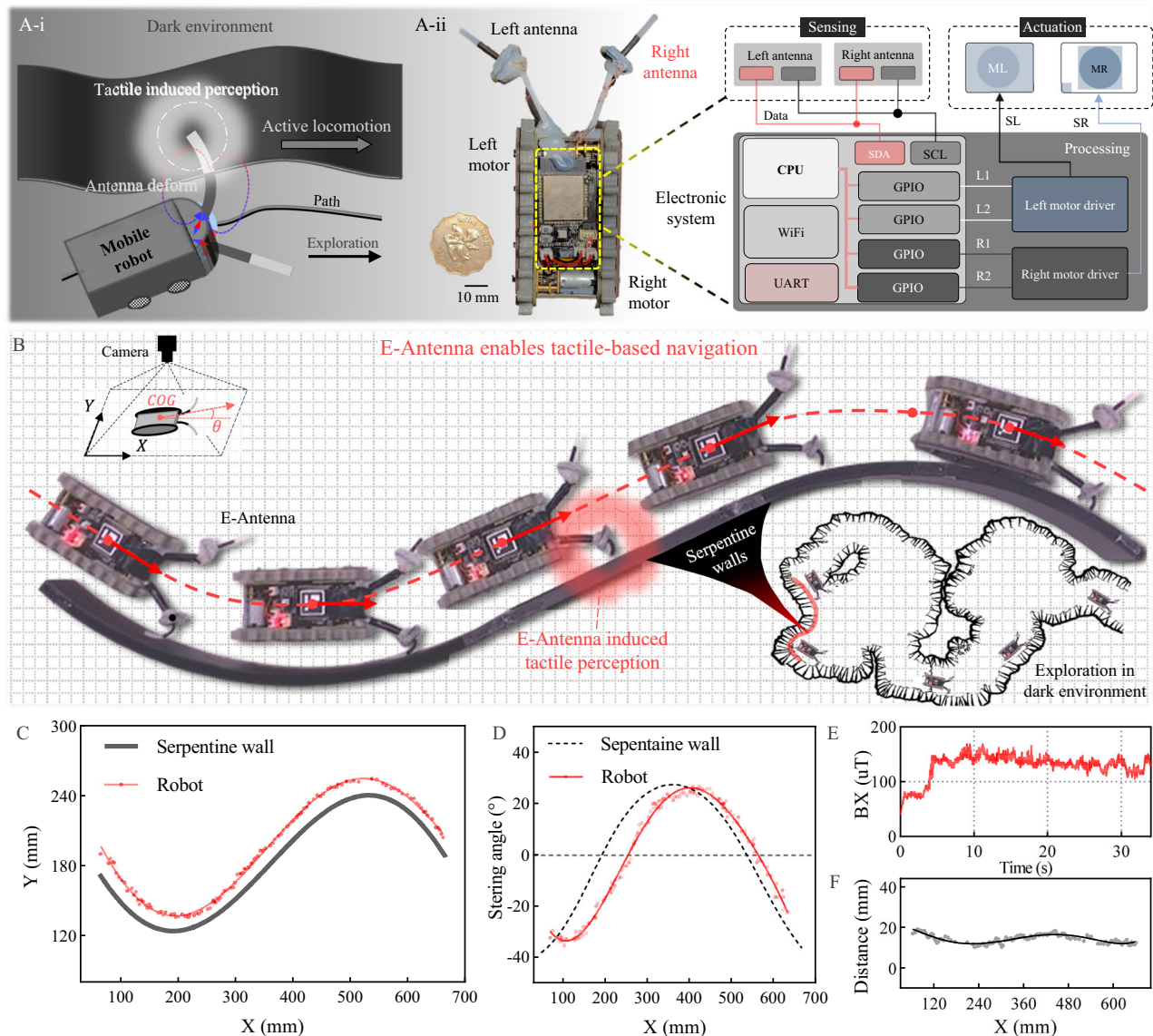


Fig. 5 | E-Antenna (centimeter-scale) enabled mobile robots to achieve insect-like vision-free wall-following navigation in the dark environment. **A-i** Schematic of tactile-based navigation in the dark environment, the E-Antenna serves as a supplemental perception source of vision in the dark environment. **A-ii** Two E-Antennas (2 mm in diameter and 20 mm in length) were mounted on both sides of a mobile robot to functionalize it with tactile perception ability. **B** Photography of insect-like vision-free wall-following navigation experiment of a small mobile robot with two E-antennas mounted on its forehead, where COG is center of gravity and θ is the steering angle. **C** The trajectory of the mobile robot (red line) during its wall-

following navigation process and the wall's serpentine outline (black line), where the moving trajectory of the mobile robot is consistent with the wall's outline. **D** The mobile robot's steering angle (labeled as red) indicates that the robot dynamically adjusts its moving direction to keep following the wall guided by the E-Antenna. **E** The raw sensing output of the E-Antenna remains stable upon contact with the wall. **F** The distance between the mobile robot and the followed wall, where the distance fluctuates within a small deviation of 2.04 mm (0.048 times the robot width).

types of flooring. Figure 6F showcases that the ATPM can effectively distinguish these floors, achieving an overall 97.33% classification accuracy (100% for carpets and ceramic tiles, and 92% for wooden floors). This underscores the E-Antenna's capability to enhance mobile robots with texture perception (Fig. S16), offering the possibility to adopt optimal strategies on different grounds, and ultimately improving their intelligence in navigation tasks such as cleaning and mapping.

Construction robots have garnered increasing attention in the industry due to their potential to solve labor shortage problems and improve working efficiency. However, it remains a challenge for robots to perform tasks requiring accurate contact sensing and perception, particularly in situations where vision cannot provide precise feedback information. One such example is conformal brushing on unknown

curved surfaces, a common task for humans but difficult for robots. The difficulty arises from the challenge of obtaining exact contact information between flexible bristles and the surface. Conventional force sensors mounted on the tool flange are unable to provide precise and direct contact information due to the force conduction distortion between flexible and rigid media.

Benefiting from the flexible structure and compact size of the E-Antenna, it can be directly embedded inside the brush's bristles, allowing it to deflect simultaneously with the bristles (Movie. S7). With the assistance of the ATPM, the E-Antenna provides precise, low-latency information about contact events and the bending states of the bristles to the robotic arm, enabling tactile-based conformal manipulation. To demonstrate this capability, we mounted the functionalized brush on a UR3e robotic arm and conducted brushing

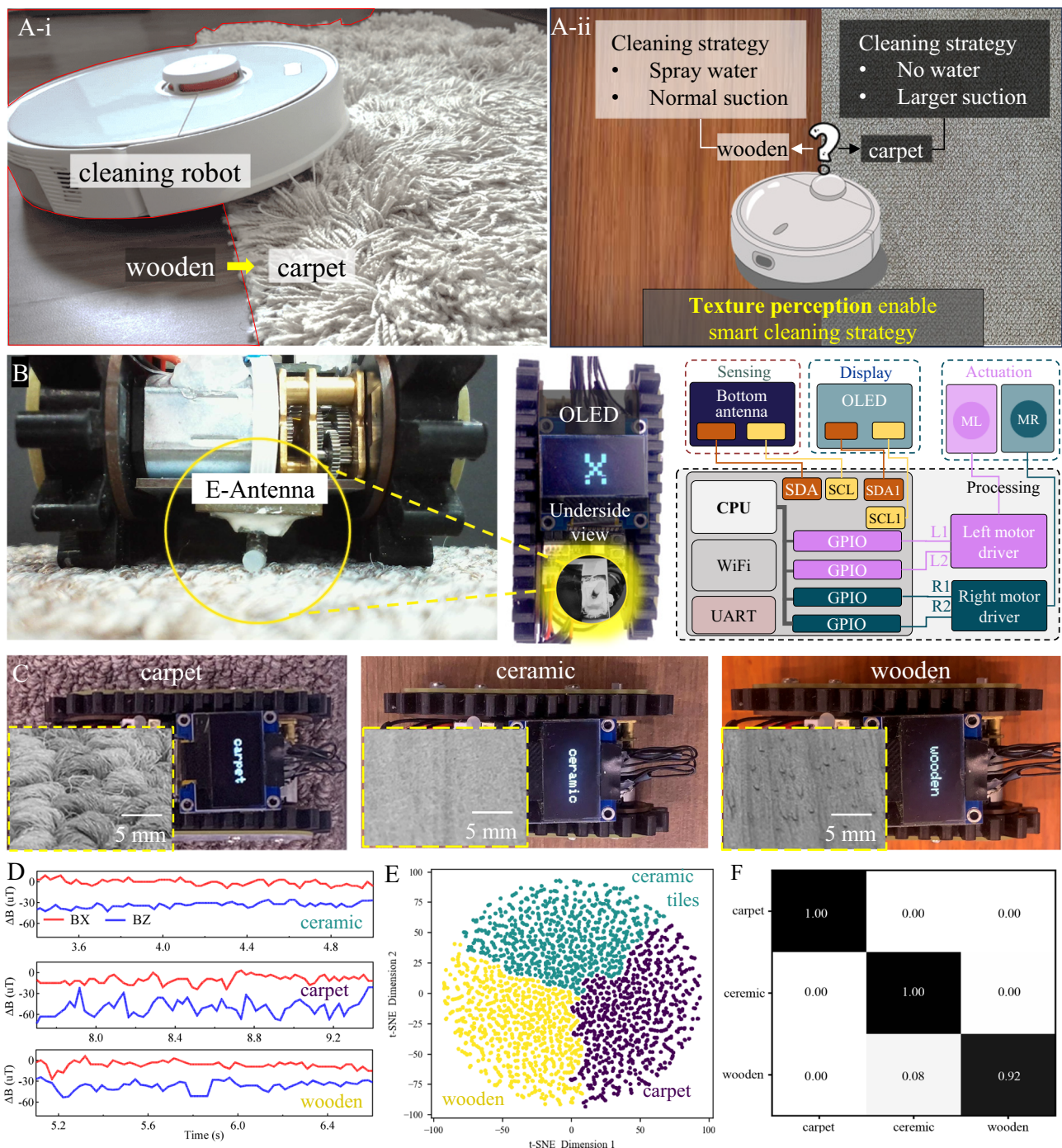


Fig. 6 | E-Antenna (millimeter-scale) enabled mobile robots with texture perception capability. **A** Functionize cleaning robots with texture perception can make them smartly adopt the adaptive cleaning strategy on different surfaces (i): a common scenario in our residential spaces with various types of floors. ii): If the existing sweeping robots have the ability of texture perception, they can choose the sweeping strategy autonomously). **B** Integrate E-Antenna (1 mm in diameter and 8 mm in length) underside of a mobile robot to functionalize it with ground texture perception capability. **C** Three common floors in residential scenes, i.e., carpet,

ceramic floor, and wooden floor, were used for testing. **D** Samples of tactile signals on these three floors show the E-Antenna can capture the fine difference between these floors. **E** Visualization of the outputs of the trained network of ATPM with t-SNE in response to these three floors, where blue dots represents the ceramic tiles, purple dots prepsents carpet, and yellow dots represents wooden. **F** Classification confusion matrix of the trained network for these three floors, where most cases achieve 100% perception accuracy, indicating that the E-Antenna can enhance the mobile robot with reliable ground perception ability.

experiments on a serpentine surface featuring three convex parts (Fig. 7A). For comparison, we also performed a control experiment without using E-Antenna's tactile feedback. The results demonstrated that the robot arm with the E-Antenna successfully maintained conformal contact and brushed all parts of the curved surface by dynamically adjusting its position and posture (Fig. 7B, C, Movie

S8). In contrast, the control group without the E-Antenna only covered 45.42% of the total area (Fig. 7D and Fig. S17).

Intriguingly, as shown in Fig. 7E, the position of the brush (red line) actually did not exactly follow the surface's outline (black line) in the successful brushing case, indicating that position control alone was insufficient for consistent conformal manipulation. The E-Antenna

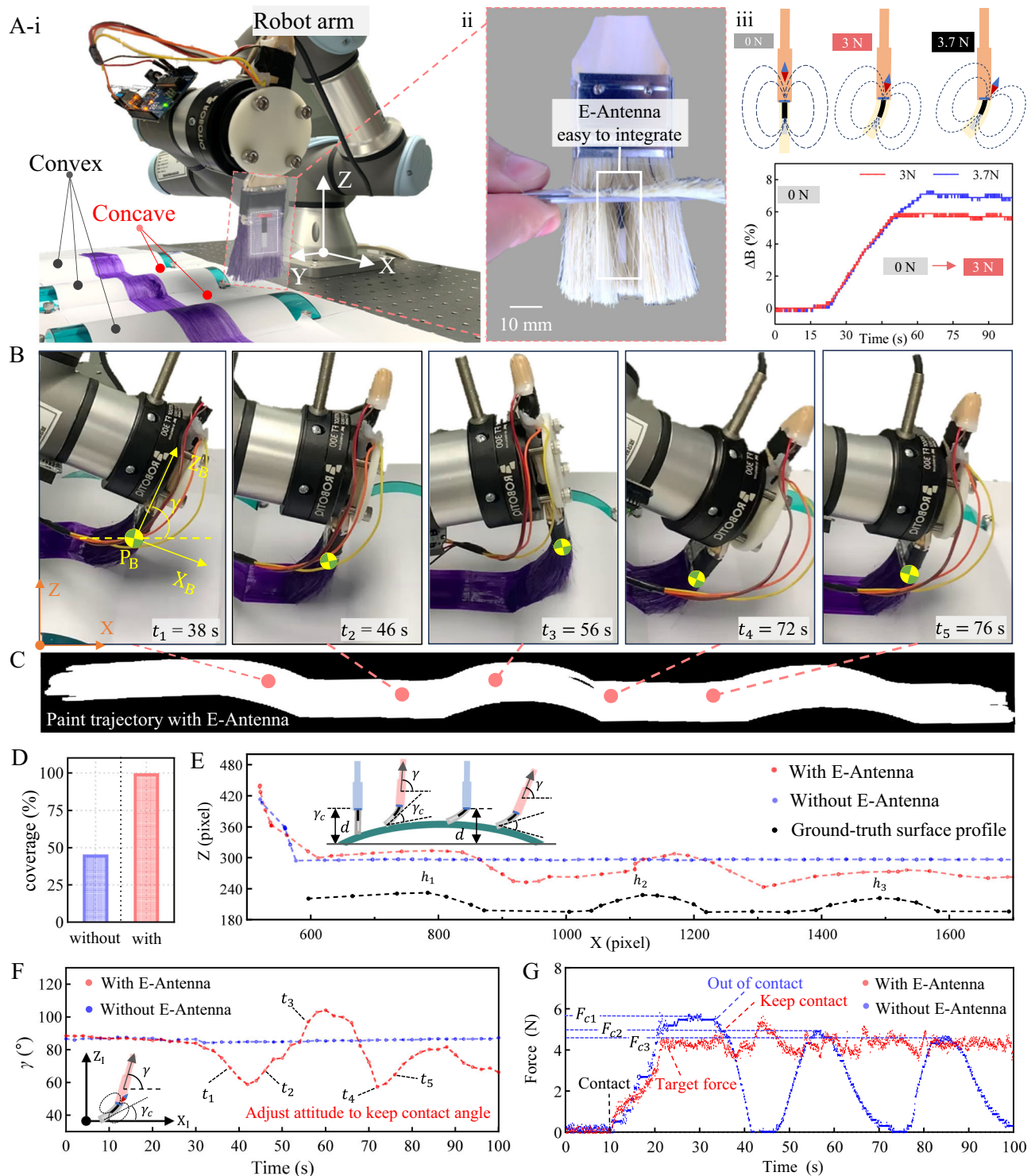


Fig. 7 | E-Antenna (larger centimeter-scale) enabled conformal painting for robot arms on curved surfaces. **A** A conformal painting experiment setup: (i) A modified brush was mounted on a robot arm to paint on a curved surface consisting of three concaves and three convexes; (ii) An E-Antenna (3 mm in diameter and 24 mm in length) was embedded into the bristles of a paintbrush to synchronously deform with it and provide tactile sensing feedback; (iii) Result of applying 3 N brushing force (labeled as red line) and 3.7 N brushing force (labeled as blue line). **B** Key frames of robot painting experiments guided by E-Antenna, where γ is the deflection angle of the brush and P_B is the position of the brush. **C** The conformal paint result. **D** Evaluation of painting coverage in these two experiments (blue represents the control experimental results without E-Antenna's feedback and red represents the experimental results with E-Antenna's feedback), where the E-Antenna

enabled conformal manipulation achieves a painting coverage of 99.92%. **E** The brush trajectories of these two comparison experiments and the surface ground truth profile (black line) recognized in image space, γ_c is the contact angle, d represents the brush's distance to the flat surface, h_1 , h_2 and h_3 represent the height of three convex part. **F** The deflection angle of the brush. In the experimental group, the brush is controlled to adaptively adjust its posture γ and position to keep the contact angle γ_c constant with the feedback of tactile information, while the brush only moved forward in the control group without E-Antenna feedback. **G** The brushing force record in these two experiments. In the experimental group, the E-Antenna offered the robot tactile information to guide it to apply constant brushing force on the curved surface, while the brushing force fluctuated obviously in the control group without the E-Antenna feedback.

perceives the deflection of the bristles and predicts their spring-back tendency from sequential changes in deflection states. This capability enables the robot to adjust both its position (Fig. 7E) and posture (γ in Fig. 7F) to maintain a stable contact angle. Furthermore, the E-Antenna enables the robot to apply the desired contact force of 4.5 N with a small overshoot of $\delta = 6.67\%$ and to maintain stability throughout the brushing process with a low variance of 0.34 N (red curve in Fig. 7G). This precise tactile sensing and perception ability offer an effective solution for robotic manipulation involving soft objects or flexible end effectors.

Discussion

Tactile sensing is indispensable for manipulation, navigation, interaction, and environmental perception in various robotic applications. While previous tactile sensors have excelled in passively detecting haptic stimuli and demonstrating precise force sensing, adaptive robotic grasp, and human-machine interaction, there still exist challenges in developing tactile sensory systems that adopt an information-seeking active strategy to enhance robots' environmental perception capabilities. Inspired by the tactile-based perception mechanism of nocturnal insects, we have designed a lightweight electronic antenna sensory system with both passive sensitive force sensing performance and AI-assisted powerful active tactile perception ability.

The design of our E-Antenna incorporates a high-aspect-ratio slender structure similar to biological antennae, resulting in good mechanical compliance and high strain sensitivity. It demonstrates exceptional mechanical robustness and resilience to physical damage, capable of recovering from 1800% twisting, 224% stretching, 300° deflection, 10^3 N compression and even needle punctures. Additionally, the segmented flexibility configuration further enhances strain sensitivity by 155.40% compared to conventional uniform flexibility configuration. Moreover, the adoption of a partial magnetization strategy further improves its magnetic sensitivity by 26.96%. Collectively, these optimized designs improve tactile sensitivity by approximately 224%, which can significantly improve the sensing SNR especially for subtle stimuli. It achieved a ~220% improvement of the SNR when sensing air flow. Furthermore, the axial magnetization design enables the E-Antenna to distinguish the direction of tactile stimuli with a maximum recognition standard deviation of 1.76° . For the optimal or the best trade-off partial magnetization ratio in specific applications (Figs. S3–4), a further analysis should be carried out to meet the unique requirement of various applications.

In comparison to planar tactile sensors, the slender cylindrical structure and elastic material construction of the E-Antenna reduce friction and increase resistance to mechanical damage when interacting with surroundings. These characteristics make it particularly suitable for actively moving to seek and gather more tactile information to achieve enhanced tactile perception. Furthermore, by integrating adjacent discrete data using a sliding window, we construct a tactile chain that retains temporal dependencies and continuities of contact events. Mimicking the biological neural-based tactile decoding mechanism, we design a sequential artificial neural network with hierarchical feature extraction and non-linear feature fusion to perceive advanced information like contact states and environmental features from the constructed tactile chain. This approach resembles insects moving their antennae to perceive surroundings and humans using their fingertips to feel surface textures, leveraging active movement to obtain a continuous tactile sequence and using the brain to extract underlying environmental information. However, in applications where providing feedback on environmental features is not required, the bioinspired computation-efficient controller³² can replace ATPM to reduce computational resource usage.

The E-Antenna can serve as a common sensor integrated with various types of platforms. We demonstrate its capability to assist a

small mobile robot to achieve biomimetic wall-following, provide ground texture recognition capability to mobiles, and enable a robot arm to achieve tactile-induced conformal manipulation on curved surfaces. In the future, it can be employed in tactile-based topography scanning, robot collision detection, robotic flexible manipulation. Additionally, with its robust resilience and sensitive omnidirectional sensing, this sensor is well-suited for integration into biomimetic robotic systems like tactile whiskers, enabling enhanced environmental perception and rich tactile data. And it also holds great potential for integration into minimally invasive surgical instruments to provide precise tactile feedback and ensure safe interaction with tissues and organs. Moreover, the E-Antenna can be incorporated with other sensors, such as vision and IMU, in the future to achieve more practical and dexterous manipulation and navigation tasks. Consequently, this research provides valuable insight into the active tactile perception of artificial tactile sensors and could be beneficial to various robotic tactile applications, such as environment perception, dexterous manipulation, and tactile-related healthcare monitoring.

Methods

Fabrication of the electronic antenna

The E-Antenna was fabricated by using a modular manufacturing approach. The artificial antenna was manufactured using only three materials, including two silicone rubbers, named Ecoflex 00-30 and DragonSkin 20 (Smooth-On, Inc.), and one permanent ferromagnetic material, specifically 5 μ m-diameter neodymium (NdFeB) powder. Firstly, we design the molds (in SolidWorks 2019) and containers for fabricating E-Antenna with targeted size (Diameter: D, Height: H, Magnetic part length: H_M , and Substrate thickness: d) (Fig. S6-I). The 3D files were exported for light 3D printing and post processing (Formlabs 3, Fig. S6-II). After that, part A and part B of DragonSkin 20 and Ecoflex 30 were mixed in a 1:1 mass ratio to obtain two suspensions, and a portion of DragonSkin 20 suspension was taken and mixed with NdFeB powder in a 1:1 mass ratio to obtain the magnetic suspension (Fig. S6-III). After removing air bubbles in a vacuum chamber, the ferromagnetic suspension was poured into a customized container A (fabricated by 3D printing, shown in Fig. S6-IV). Then, the molds A and B were assembled together and subsequently pressed into container A to fill the void with the ferromagnetic suspension (Fig. S6-V). After curing at 60°C for two hours, the grouped mold was pressed into container B with Ecoflex suspension to fabricate the substrate of the antenna (Fig. S6-VI-VII). At the same time, mold A was removed (Fig. S6-VIII) and filled with pure DragonSkin suspension to obtain the non-ferromagnetic segment (Fig. S6-IX). After curing at 60°C for two hours, mold B and container B were removed (Fig. S6-X), and the antenna array was magnetized along the axial direction by a pulse magnetizing machine to obtain the flexible antenna array (Fig. S6-XI, Fig. S8). Finally, an antenna was clipped (Fig. S6-XII) and assembled on a tiny Hall sensor (MLX90393, Melexis, Inc.) to form an E-Antenna (Fig. 1B).

Electronic system design, fabrication and programming

Two schemes for reading sensors were presented in this study: a popular commercial Arduino UNO board and a customized wireless tiny electronic board with a size of 22 × 40 × mm (support WIFI and BLE 5.0 communication protocol). The block diagram and 3D view of the customized board are provided in Fig. S18. The fabrication and SMT assembly were performed by JLC Technology. All components were sourced from Digi-Key electronics, including the microprocessor ESP32-S3-WROOM-1 module (Espressif Systems, Inc.), low quiescent current low-dropout (LDO) regulator (SY8089A1AAC, Silergy Corp), a FPC connector (FH34SRJ-4S-0.5SH(50), HRS), two brushed DC motor drivers for the mobile robot (DRV8837DSGR, Texas Instruments), and a USB-to-UART chip (CH340N). The firmware was downloaded into the MCU in its UART download boot mode. The integrated development

environment (IDE) used in this project is Arduino IDE (2.0.4 version). Part of the firmware was modified based on an open-source MLX90393 driver (Written by Kevin Townsend for Adafruit Industries. MIT license) and development kit (SDK) provided by Espressif Systems.

Sensor characterization and sensing test platform

The E-Antenna was characterized on a manual displacement platform and an automatic moving platform. The manual moving platform consists of a three-axis precision displacement platform (LD-60) with a step displacement of 10 μm , a porous aluminum alloy mounting base (OHD-6C15, Oeabt Optics), several cross-fixed frames and various stainless steel shafts, was used to characterize the static response of the E-Antenna under various loads. A force sensor (HP-2, HANDPI) with a force-sensing precision of 0.001 N was mounted through a stainless steel shaft and served as the ground truth of the loads, the assembly photos are shown in Fig. S7. The automatic moving platform consists of a two-axis linear moving platform and a rotating platform. The linear motion platform was constructed with two linear screw guide rails with a high translational precision of 10 μm (screw diameter 6 mm, screw pitch 1 mm, motor type: NEMA11 stepper motor with a 28 \times 28 mm faceplate and 1.8° step angle). The rotating platform was actuated by a stepper motor with a step angle of 0.9°. The 3D-printed probe is mounted on the two-axis moving platform to apply loads, and the force sensor (HP-2, HANDPI) with a force-sensing precision of 0.001 N was used as the ground truth of the loads. Three stepper motor drivers (LC42H240, LiCHUAN) were programmed by Arduino Mega 2560 through the common anode connection pattern to control stepper motors in the test platform. This platform was used to apply loads with different directions, dynamic loads with different amplitudes, patterns, and frequencies, as well as thousands of repeated constant loads to the antenna for verifying its sensing performance and consistency.

Tactile perception dataset building

Tactile perception datasets were built to train the ATPM for various tactile perception tasks. For the curved surface perception demonstration, we prepared five customized 3D-printed samples made of the same material with different curvatures. For the ground texture perception demonstration, we selected three kinds of floors that are commonly used in homes, including ceramic tile, wooden floors, and carpets. The E-Antenna was mounted on the linear moving platform to slide across these samples to collect dynamic tactile data repeatedly for building train datasets. In the surface curvature recognition experiment, the process was divided into six stages according to antenna states: the reaching stage S0, the initial contact stage S1, sliding on noncurved part S2, slow springback stage S3, rapid springback stage S4, and complete springback stage S5. The index of these six stages as well as the ground-truth curvature were saved as the labels of the dataset. In the ground texture recognition experiment, the ground-truth floor type was saved as the labels of the dataset. The dataset size is 2500, and was split into training, validation, and testing sets as follows: 7:2:1. For classification, we utilized the well-trained ATPM based on multilayer LSTM sequential model, with the following key parameters: Input layer: the sequence length is 12, each element is 2 dimensions; Bi-directional LSTM layer: input size is 2, hidden size is 12, layer is 2, batch size is 10; Unidirectional LSTM layer: input size is 2 \times 12, hidden size is 12, layer is 1, batch size is 10; Full contact layer1: input size is 12, output size is 5; Full contact layer2: input size is 12, output size is 6; The epoch number is 2000, learning rate is 0.001, loss function is Cross Entropy Loss, optimizer is Adam.

Demonstration setup

For the conformal painting manipulation task, an E-Antenna (diameter: 2 mm, length: 20 mm) was first embedded into the bristles of a paintbrush. The sensing signals were acquired by the Arduino UNO via

IIC protocol and were transmitted to a computer via USB to a laptop to control the robot arm via TCP/IP.

For the wall-following navigation task, two E-Antennas (diameter: 2 mm, length: 20 mm) were mounted on the head of a tiny mobile robot (40 \times 80 \times 30 mm). The block diagram of a revised mobile robot system is presented in Fig. 6B. The tactile signals were acquired by a customized circuit board (23 \times 40 \times 2 mm) via IIC protocol and wirelessly transmitted to the laptop via BLE 5.1 protocol (details were included in Fig. S19).

For the ground texture perception task, one E-Antenna (diameter: 0.8 mm, length: 10 mm) was mounted on the underside of another mobile robot. Besides, a 0.96-inch OLED screen (HS96L03W2C03) was integrated as the display interface. The block diagram of the whole system is shown in Fig. 6. The tactile signals were acquired by the customized circuit board via IIC protocol and wirelessly transmitted to the laptop via BLE 5.1 protocol.

The data-receiving system on the computer was developed with Python 3.8. An open-source cross-platform BLE client library (bleak 0.21.1, Copyright (c) 2020, Henrik Blidh) was used to connect to and receive data from the E-Antenna system acting as the GATT server. In addition, by using multiple threads for reading, processing, and data saving in parallel, the final average sampling frequency of the wireless host system is ~50 Hz.

Data availability

All the data supporting the findings of this study are available within this article and its Supplementary Information. Any additional information can be obtained from corresponding authors upon request. Source data are provided with this paper.

Code availability

All codes used in this study are available at code ocean (<https://doi.org/10.24433/CO.3143395.v2>).

References

1. Liu, Z. et al. A three-dimensionally architected electronic skin mimicking human mechanosensation. *Science* **384**, 987–994 (2024).
2. Yu, Y. et al. All-printed soft human-machine interface for robotic physicochemical sensing. *Sci. Robot.* **7**, eabn0495 (2022).
3. Boutry, C. M. et al. A hierarchically patterned, bioinspired e-skin able to detect the direction of applied pressure for robotics. *Sci. Robot.* **3**, eaau6914 (2018).
4. He, Y., Cheng, Y., Yang, C. & Guo, C. F. Creep-free polyelectrolyte elastomer for drift-free iontronic sensing. *Nat. Mater.* **23**, 1107–1114 (2024).
5. Liu, F. et al. Printed synaptic transistor-based electronic skin for robots to feel and learn. *Sci. Robot.* **7**, eabl7286 (2022).
6. Yan, Y. et al. Soft magnetic skin for super-resolution tactile sensing with force self-decoupling. *Sci. Robot.* **6**, eabc8801 (2021).
7. Zheng, Q. et al. Towards a sustainable monitoring: a self-powered smart transportation infrastructure skin. *Nano Energy* **98**, 107245 (2022).
8. Qu, X. et al. Artificial tactile perception smart finger for material identification based on triboelectric sensing. *Sci. Adv.* **8**, eabq2521 (2022).
9. Ward-Cherrier, B. et al. The tactip family: soft optical tactile sensors with 3d-printed biomimetic morphologies. *Soft Robot.* **5**, 216–227 (2018).
10. Bai, H. et al. Stretchable distributed fiber-optic sensors. *Science* **370**, 848–852 (2020).
11. Su, Q. et al. A stretchable and strain-unperturbed pressure sensor for motion interference-free tactile monitoring on skins. *Sci. Adv.* **7**, eabi4563 (2021).

12. Liu, F. et al. Neuro-inspired electronic skin for robots. *Sci. Robot.* **7**, eabl7344 (2022).
13. Djenoune, L. et al. Cilia function as calcium-mediated mechanosensors that instruct left-right asymmetry. *Science* **379**, 71–78 (2023).
14. Katoh, T. A. et al. Immobile cilia mechanically sense the direction of fluid flow for left-right determination. *Science* **379**, 66–71 (2023).
15. Chapman, T. & Webb, B. A model of antennal wall-following and escape in the cockroach. *J. Comp. Physiol. A* **192**, 949–969 (2006).
16. Zheng, X., Kamat, A. M., Krushynska, A. O., Cao, M. & Kottapalli, A. G. P. 3D Printed Graphene Piezoresistive Microelectromechanical System Sensors to Explain the Ultrasensitive Wake Tracking of Wavy Seal Whiskers. *Adv. Funct. Mater.* **32**, 2207274 (2022).
17. Nguyen, N. H. & Ho, V. A. Mechanics and morphological compensation strategy for trimmed soft whisker sensor. *Soft Robot.* **9**, 135–153 (2022).
18. Emnett, H., Graff, M. & Hartmann, M. A novel whisker sensor used for 3d contact point determination and contour extraction. In *Proc. of Robotics: Science and Systems*. (RSS) (2018).
19. Massari, L. et al. A machine-learning-based approach to solve both contact location and force in soft material tactile sensors. *Soft Robot.* **7**, 409–420 (2020).
20. Kim, S., Velez, C., Patel, D. K. & Bergbreiter, S. in *2019 IEEE/RSJ International Conference on Intelligent Robots and Systems (IROS)*. (IEEE, 2019).
21. Gomez, V., Remmas, W., Hernando, M., Ristolainen, A. & Rossi, C. Bioinspired whisker sensor for 3D mapping of underground mining environments. *Biomimetics* **9**, 83 (2024).
22. Alfadhel, A. & Kosel, J. Magnetic nanocomposite cilia tactile sensor. *Adv. Mater.* **27**, 7888–7892 (2015).
23. Diamond, M. E., Von Heimendahl, M., Knutsen, P. M., Kleinfeld, D. & Ahissar, E. ‘Where’ and ‘what’ in the whisker sensorimotor system. *Nat. Rev. Neurosci.* **9**, 601–612 (2008).
24. Cowan, N. J., Lee, J. & Full, R. J. Task-level control of rapid wall following in the American cockroach. *J. Exp. Biol.* **209**, 1617–1629 (2006).
25. Mongeau, J.-M., Demir, A., Lee, J., Cowan, N. J. & Full, R. J. Locomotion-and mechanics-mediated tactile sensing: antenna reconfiguration simplifies control during high-speed navigation in cockroaches. *J. Exp. Biol.* **216**, 4530–4541 (2013).
26. Saltin, B. et al. Material stiffness variation in mosquito antennae. *J. R. Soc. Interface* **16**, 20190049 (2019).
27. Yu, Y. S., Graff, M. M., Bresee, C. S., Man, Y. B. & Hartmann, M. J. Whiskers aid anemotaxis in rats. *Sci. Adv.* **2**, e1600716 (2016).
28. Chen, L. et al. Spike timing–based coding in neuromimetic tactile system enables dynamic object classification. *Science* **384**, 660–665 (2024).
29. Nogueira, R., Rodgers, C. C., Bruno, R. M. & Fusi, S. The geometry of cortical representations of touch in rodents. *Nat. Neurosci.* **26**, 239–250 (2023).
30. Wijnjtes, M. W., Sato, A., Hayward, V. & Kappers, A. M. Local surface orientation dominates haptic curvature discrimination. *IEEE Trans. Haptics* **2**, 94–102 (2009).
31. Lee, M. M. Tactile sensors need a greater sense of purpose. *Sci. Robot.* **7**, eabn9086 (2022).
32. Webster-Wood, V. A., Gill, J. P., Thomas, P. J. & Chiel, H. J. Control for multifunctionality: bioinspired control based on feeding in *Aplysia californica*. *Biol. Cybern.* **114**, 557–588 (2020).

Acknowledgements

This work was funded by Hong Kong RGC General Research Fund (16203923), National Natural Science Foundation of China/Research Grants Council Joint Research Scheme (N_HKUST638/23, 62361166630), and Guangdong Basic and Applied Basic Research Foundation (2023B1515130007).

Author contributions

Conceptualization, Y.S. and H.R.; methodology, H.R. and L.Y.; software, H.R. and H.C.; validation, H.R., Y.L., H.C., T.Z., G.L., X.Y., and Y.T.; formal analysis, H.R. and L.Y.; data curation, H.R., L.Y., H.C.; visualization, H.R., L.Y.; writing - original draft preparation, G.R.; writing - review and editing, H.R. and Y.S.; supervision, Y.S.; project administration, W.S. and Y.S.; funding acquisition, W.S. and Y.S. All authors have read and agreed to the published version of the manuscript.

Competing interests

The authors declare no competing interests.

Additional information

Supplementary information The online version contains supplementary material available at <https://doi.org/10.1038/s41467-025-58403-3>.

Correspondence and requests for materials should be addressed to Yajing Shen.

Peer review information *Nature Communications* thanks Juan Wachs, Emanuele Lindo Secco and the other, anonymous, reviewer(s) for their contribution to the peer review of this work. A peer review file is available.

Reprints and permissions information is available at <http://www.nature.com/reprints>

Publisher’s note Springer Nature remains neutral with regard to jurisdictional claims in published maps and institutional affiliations.

Open Access This article is licensed under a Creative Commons Attribution-NonCommercial-NoDerivatives 4.0 International License, which permits any non-commercial use, sharing, distribution and reproduction in any medium or format, as long as you give appropriate credit to the original author(s) and the source, provide a link to the Creative Commons licence, and indicate if you modified the licensed material. You do not have permission under this licence to share adapted material derived from this article or parts of it. The images or other third party material in this article are included in the article’s Creative Commons licence, unless indicated otherwise in a credit line to the material. If material is not included in the article’s Creative Commons licence and your intended use is not permitted by statutory regulation or exceeds the permitted use, you will need to obtain permission directly from the copyright holder. To view a copy of this licence, visit <http://creativecommons.org/licenses/by-nc-nd/4.0/>.

© The Author(s) 2025